Available online at www.sciencedirect.com
ScienceDirect
Journal of Hazardous Materials 153 (2008) 514–524
Journal of Hazardous Materials
www.elsevier.com/locate/jhazmat

# Characterization, morphology and composition of biofilm and precipitates from a sulphate-reducing fixed-bed reactor

Emmanouela Remoundaki [a,*], Pavlina Kousi [a], Catherine Joulian [b], Fabienne Battaglia-Brunet [b], Artin Hatzikioseyian [a], Marios Tsezos [a]

[a] *National Technical University of Athens, School of Mining and Metallurgical Engineering, Laboratory of Environmental Science and Engineering, Heroon Polytechniou 9, 15780 Athens, Greece*
[b] *BRGM, Environment and Process Division, Biotechnology Unit, 3 Avenue Claude Guillemin, 45060 Orleans Cedex 2, France*

Received 5 June 2007; received in revised form 28 August 2007; accepted 29 August 2007
Available online 4 September 2007

**Abstract**

The characteristics of the biofilm and the solids formed during the operation of a sulphate-reducing fixed-bed reactor, fed with a moderately acidic synthetic effluent containing zinc and iron, are presented. A diverse population of δ-*Proteobacteria* SRB, affiliated to four distinct genera, colonized the system. The morphology, mineralogy and surface chemistry of the precipitates were studied by X-ray diffraction (XRD), scanning electron microscopy (SEM) and energy dispersive X-ray (EDX). The XRD patterns observed are characteristic of amorphous solid phases. Peaks corresponding to crystalline iron sulphide, marcasite, sphalerite and wurtzite were also identified. SEM–EDX results confirm the predominance of amorphous phases appearing as a cloudy haze. EDX spectra of spots on the surface of these amorphous phases reveal the predominance of iron, zinc and sulphur indicating the formation of iron and zinc sulphides. The predominance of these amorphous phases and the formation of very fine particles, during the operation of the SRB column, are in agreement and can be explained by the formation pathways of metal sulphides at ambient temperature, alkaline pH and reducing conditions. Solids are precipitated either as (i) amorphous phases deposited on the bed material, as well as on surface of crystals, e.g. $Mg_3(PO_4)_2$ and (ii) as rod-shaped solids characterized by a rough hazy surface, indicating the encapsulation of bacterial cells by amorphous metal sulphides.


*Keywords:* Sulphate-reducing bacteria; Fixed-bed reactor; Amorphous phases; Zinc sulphides; Iron sulphides; *dsr*AB gene diversity

## 1. Introduction

Wastewater originating from mining and metallurgical industries is often acidic and typically characterized by a significant content of sulphates and soluble metals, such as Zn, Fe, Cu, Ni, Pb and Cd. Soluble metal- and sulphate-bearing wastewater treatment schemes are usually based on sulphate-reducing reactors recently developed in both pilot and full scale [1–8]. The operation of the sulphate-reducing reactors is based on (1) the exclusion of oxygen, (2) the presence of sulphates in the wastewater under treatment, (3) the establishment of a sulphate-reducing bacteria population, either indigenous or introduced, (4) a source of simple organic compounds to serve as carbon source for bacterial growth and (5) a way to retain metal sulphide precipitates.

In such reactor schemes, sulphate-reducing bacteria (SRB) [9] oxidize simple organic compounds, such as lactic acid [10], under anaerobic conditions, transforming the sulphates combined in the wastewater into hydrogen sulphide while generating bicarbonate ions:

$$2CH_3CH(OH)COOH + 3SO_4^{2-} \rightarrow 3H_2S + 6HCO_3^- \quad (1)$$

Hydrogen sulphide reacts with the present divalent soluble metals which are then sequestered from wastewater as insoluble metal sulphides in the form of various mineral phases [6,11,12]:

$$H_2S + Me^{2+} \rightarrow MeS_{(s)} + 2H^+ \quad (2)$$

where Me stands for metals such as Zn, Fe, Cu, Ni, Pb, Cd, etc.

* Corresponding author. Tel.: +30 210 772 2271; fax: +30 210 772 2173.
*E-mail address:* remound@metal.ntua.gr (E. Remoundaki).

0304-3894/$ – see front matter © 2007 Elsevier B.V. All rights reserved.
doi:10.1016/j.jhazmat.2007.08.094

Bicarbonate ions react with protons to form $CO_2$ and water; thus, removing acidity from solution as $CO_2$:

$$HCO_3^- + H^+ \rightarrow CO_{2(g)} + H_2O \quad (3)$$

$H_2S$ and $HCO_3^-$ formed during sulphate reduction equilibrate into a mixture of $H_2S$, $HS^-$, $S^{2-}$, $CO_2$, $HCO_3^-$ and $CO_3^{2-}$. This mixture buffers the solution pH typically around neutral to slightly alkaline values [1]. The shift of the pH of the acidic solution towards neutral to slightly alkaline values may also lead trivalent metals, such as Al, Fe and Cr, to hydrolyze and precipitate as insoluble hydroxides or oxides. Highly soluble oxyanions, such as chromate, selenate, molybdate and uranyl-carbonate complexes, can also be successfully sequestered from wastewater when treated in sulphate-reducing reactors by reduction, thanks to the reducing, electron-rich environment of the reactor, and precipitated as hydroxides/oxides due to the alkalinity generated by the bacterial metabolism [13]. Metals complexed with ammonia or cyanide are also more readily precipitated as sulphides than as hydroxides [14].

Apart from the obvious advantage of simultaneous substantial reduction of the concentrations of metals and sulphates effected by the treatment of wastewater in sulphate-reducing reactors, sulphide precipitation has several additional potential advantages. Metal sulphides are generally less soluble than their corresponding metal hydroxides; allowing quantitative metal precipitation [15,16]. Metal sulphides are also more compact, have faster settling velocities and exhibit better thickening and dewatering characteristics than the corresponding hydroxide sludge [17]. Metal sulphide volume is 6–10 times lower than metal hydroxide/gypsum sludge from conventional neutralization [8]. Despite the advantages mentioned above, the objectionable odour and toxicity of $H_2S$ as well as the fate of the sludge produced are issues often addressed for technology improvement.

The study of the composition and the characteristics of the solids produced by the operation of a sulphate-reducing reactor is necessary in order to better understand the main mechanisms involved and their relative importance for (i) operating conditions definition, (ii) efficiency improvement and (iii) safer operation. Moreover, the information acquired by the study of the solids composition and their characteristics is necessary for the decisions to be taken about the fate of the sludge produced, dealing with options such as further treatment of the sludge for metal recovery or disposal of the untreated sludge [18].

The present paper summarizes the results obtained from the study of the morphology and composition of the biofilm and the precipitates formed during 1 year of continuous operation of a sulphate-reducing fixed-bed reactor treating metal-bearing, sulphate-rich simulated wastewater.

## 2. Materials and methods

### 2.1. Sulphate-reducing fixed-bed reactor

The sulphate-reducing fixed-bed reactor, operating in upflow mode, is presented in Fig. 1. The biofilm was established on porous sintered glass spheres with average diameter of 1 cm and 1500 $m^2$/L specific surface area. This material has the advantage of a very large surface area, available for biofilm development.

Sludge from the anaerobic digestion tank of a wastewater treatment plant (Municipal Wastewater Treatment Plant, Metamorphosi, Athens) was used as inoculum for the development of a mixed, sulphate-reducing culture.

The reactor was fed with a variation of Postgate's medium (DSMZ, *Desulfovibrio* medium, Medium 63). This nutrient

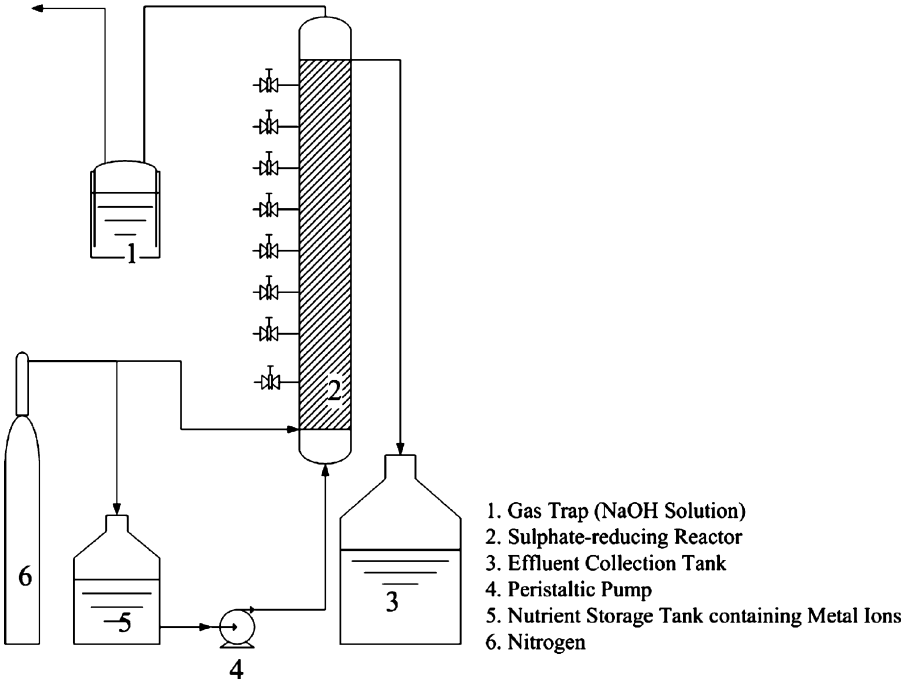


Fig. 1. Sulphate-reducing fixed-bed reactor. Height: 1 m, diameter: 9.5 cm, bed height: 82 cm and head space (necessary for gas collection and removal): 18 cm.

is typically used for SRB cultures [3–6,19]. The composition of the nutrient medium is (all in g/L), DL-Na-lactate (50%), 4.0; yeast extract, 1.0; $Na_2SO_4$, 1.0; $MgSO_4{\cdot}7H_2O$, 2.0; $FeSO_4{\cdot}7H_2O$, 0.5; $NH_4Cl$, 1.0; $K_2HPO_4$, 0.5; $CaCl_2{\cdot}2H_2O$, 0.1; Na-thioglycolate, 0.1; ascorbic acid, 0.1; resazurin, 0.001.

The reactor operated first for a period of 35 days in batch mode (close loop) for biofilm establishment with periodic replacement of the nutrient medium. Apart from the permanent characteristic odour of the produced hydrogen sulphide and the black colour of the beads of the column bed, the establishment of the biofilm was indirectly checked by the systematic pH monitoring of the liquid phase (neutral pH values) and the analytical determination of sulphate concentrations. Following the first days of operation in batch mode, sulphates were reduced to a satisfactory percentage of 80% of the initial sulphate concentration fed to the reactor. Following the period of biofilm establishment, the reactor was operated in continuous mode, fed with synthetic solutions containing the nutrient medium supplemented with ferrous iron sulphate (100 mg/L Fe) and increasing zinc sulphate (50–400 mg/L Zn) concentrations [20]. The pH of the feed solutions was adjusted to 3–4 by addition of HCl (Merck, analytical grade).

The reactor operated continuously for 310 days at room temperature (mean temperature 22 °C) and hydraulic retention time (HRT) values ranging between 2 and 10 h. In order to study the influence of initial sulphate, organic carbon, iron and zinc concentrations on the reactor efficiency, a constant HRT value of 9 h was selected [20].

### 2.2. Liquid phase monitoring

During the operation of the reactor, sampling was systematically performed at the following points: inlet, outlet and eight different equally spaced sampling ports along the column length. The liquid phase samples were vacuum filtered through 0.22 μm sterilized membranes (Gelman) before any analytical determination. Analytical methodology and results concerning the liquid phase monitoring are presented elsewhere [20].

### 2.3. Solid samples

#### 2.3.1. Bacterial population characterization

The fingerprinting capillary electrophoresis single strand conformational polymorphism (CE-SSCP) technique [21] was used to check the stability of the bacterial population along the column bed. Effluent samples were collected twice: the first sampling set nominated as A was collected at week 26 of the reactor operating period. The second set nominated as B was collected a week later. Both sets of effluent samples were collected from three sampling ports: (1) the first port by the bottom of the column-influent (1A/1B), (2) the port located in the middle of the bed (5A/5B) and (3) the last port coinciding with the outlet of the column-effluent (8A/8B). It is important to point out that systematic pH profiles, obtained during the operation of the reactor along the column bed, indicated that the pH always reaches a value around 8 within the first 10 cm (the first port by the bottom of the column) of the column bed as a result of the alkalinity generated during the SRB metabolism [20]. A volume of 10 mL of each sample was vacuum filtered under sterile conditions through 0.22 μm sterile membranes and was kept under aseptic conditions until treatment.

Bacterial genomic DNA was extracted from the material retained on the filters by bead beating using the Bio101 FastPrep Instrument and the FastDNA Spin Kit for Soil (Bio101, Vista, CA, USA). About 200 bp of the V3 region of the 16S rRNA genes of members of the *Bacteria* domain were PCR amplified from DNA extracts with the eubacterial forward primer w49 (5′-ACGGTCCAGACTCCTACGGG-3′; *Escherichia coli* position, 331) and the universal reverse primer w34 (5′-TTACCGCGGCTGCTGGCAC-3′; *E. coli* position, 533) 5′ end-labelled with the fluorescent dye FAM.

PCR products were 100-fold diluted in nuclease-free water so that fluorescence did not exceed the maximum of the software during CE-SSCP analyses, and 1 μL of diluted PCR product was added to a mixture of 18.8 μL of deionized formamide and 0.2 μL of Genescan-500 LIZ internal standard (Applied Biosystems). To obtain single-strand DNA, samples were heat denatured for 5 min at 95 °C and immediately cooled on ice. CE-SSCP electrophoresis was performed at 12 kV and at 32 °C in an ABI Prism 310 genetic analyzer using a 47 cm length capillary filled with non-denaturing 5.6% CAP polymer (Applied Biosystems). Raw data analyses and assignment of peak position were done with the software GeneScan (Applied Biosystem).

SRB diversity was specifically investigated in the bottom and the middle of the bed, using primers DSR1F (5′-ACSCACTGGAAGCACG-3′) and DSR4R (5′-GTGTAGCAGTTACCGCA-3′) targeting partial α- and β-subunits of the dissimilatory sulphite reductase (*dsr*AB) genes (ca. 1.9 kb), encoding a key enzyme involved in sulphate reduction. PCR products were gel purified (Geneclean Turbo kit, Qbiogen, Montreal, Canada) and ligated into pCR®4-TOPO® plasmids (Invitrogen). Right-length inserts were clustered into Operating Taxon Unit (OTU) depending on their *Rsa*I restriction profiles. After purification (NucleoSpin Multi 8 Plus kit, Macherey Nagel), one clone of each OTU was sent to Genome Express (Grenoble, France) for sequencing of the insert with primers specific to the plasmid.

Amino-acid (deduced from nucleotidic sequences of *dsr*AB genes) sequences were aligned with reference sequences obtained from GenBank [22] using the sequence alignment editor BioEdit [23]. Pairwise evolutionary distances of ca. 500 unambiguous amino acids of the DsrAB were computed by the method of [24].

*dsr*AB gene sequences have been deposited in GenBank under accession numbers EF645664 to EF645676.

#### 2.3.2. Carbon, sulphur and metals determination in solids

Bulk solid samples were collected by sedimentation of the suspended solids contained in the reactor effluent. The samples were centrifuged and the separated solids were ground, dried at 105 °C and kept in a desiccator prior to any of the following determinations: loss on ignition at 550 °C, carbon and sulphur content by LECO, iron and zinc determination by ICP following acid digestion of the samples.

*2.3.3. Mineralogical analysis by X-ray diffraction*

Powder XRD analysis of the bulk solid samples was performed on a Siemens D5000 X-ray diffractometer. The samples were step scanned from 2° to 80° (2$\theta$), at a step of 0.02° and step time of 1 s.

*2.3.4. Solids morphology and surface semi-quantitative chemical analysis by SEM coupled with EDX*

The solids morphology study was performed using a scanning electron microscope (Fei Quanta 200) in low-vacuum (20 kV) mode on non-coated material. Semi-quantitative elemental analysis of the SEM samples was carried out by energy dispersive X-ray spectrometry (EDX system by EDAX) operating at an accelerating potential of 20 kV and a probe current of 3–6 nA, employing a link analytical EDX system.

Samples of glass beads taken from the fixed bed of the column before and after the establishment of the biofilm and the precipitation of solids as well as filter membranes (0.22 μm) from the liquid filtrates charged with the solids retained from the different sampling ports of the column reactor have been subjected to SEM–EDX analysis.

## 3. Results and discussion

### *3.1. Bacterial population*

Complex molecular fingerprints of 16S rRNA genes were obtained, showing that a diverse bacterial community established along the column bed (Fig. 2). For each one of the three samples corresponding to a sampling port, the results obtained for both sample sets A and B gave almost identical fingerprints showing high reproducibility (Fig. 2). Moreover, the fingerprints presented in Fig. 2 reveal that the community colonizing the middle bed was identical to the community retrieved at the outlet of the column. Fingerprints were slightly different at the bottom bed, although same peaks were detected. These results show that the community, although complex, had thus reached a steady state.

The diversity of SRB at the bottom and the middle part of the column bed was specifically investigated by using *dsr*AB genes encoding a key enzyme involved in dissimilatory sulphate reduction. A diverse population of δ-*Proteobacteria* SRB affiliated to four distinct genera colonized the system. A species of the genus *Desulfomicrobium* and the species *Desulfobacter postgatei* were detected at both locations. In addition, two species of the genus *Desulfovibrio* were found only at the bottom part of the bed, whereas two species of the genus *Desulfobulbus* and another *Desulfomicrobium*-like bacterium developed in the middle part of the bed.

The availability of lactate in the nutrient medium, a common substrate to many sulphate reducers, probably explains the detection of such diverse population of SRB in the bioreactor. This compound is however not used by some SRB, including several species of *Desulfobacter*, *Desulfotomaculum acetoxidans* and some species of *Desulfobacterium* [25]. Similarly to our findings, Kaksonen et al. [5,19] could detect, among other organisms, strains phylogenetically related to *Desulfovibrio* and

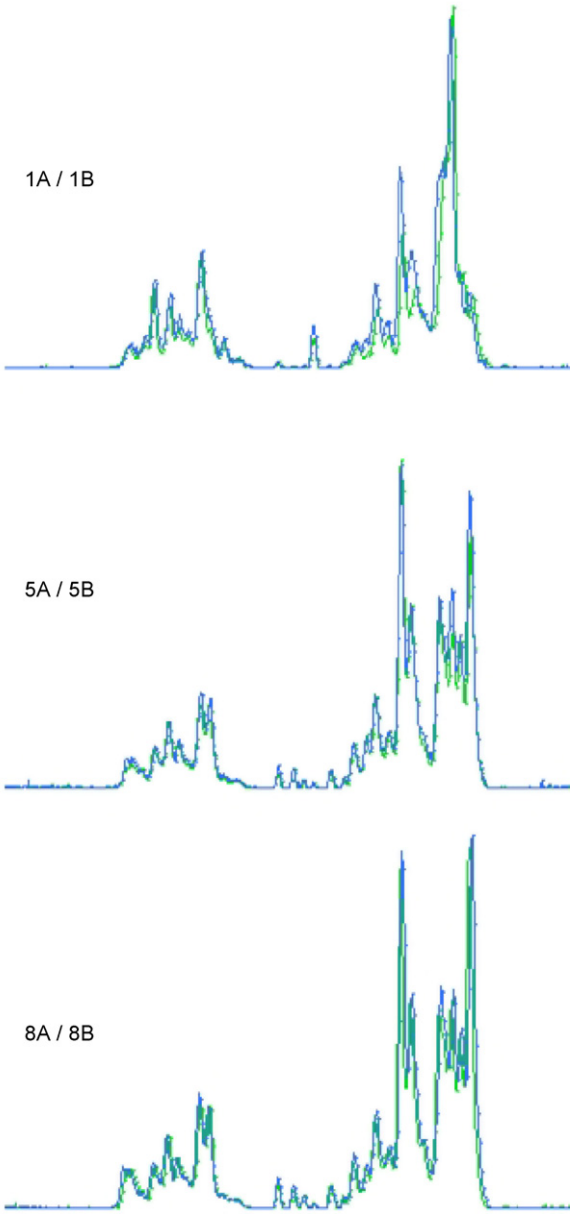


Fig. 2. Molecular CE-SSCP fingerprints of 16S rRNA genes of the bacterial community colonizing the column bed for two sets of samples (A and B). 1A/1B samples from the reactor inflow, 5A/5B samples from the middle of the bed and 8A/8B samples from the reactor outflow.

*Desulfobulbus* in a lactate-fed fluidized-bed reactor (effluent pH ranging from 7 to 8) treating acidic metal-containing wastewater, using 16S rRNA gene clone libraries and culturing techniques. Dar et al. [26] also detected bacteria belonging to *Desulfovibrio* and *Desulfobulbus* genera in sulfidogenic bioreactors (effluent pH ranging from 7 to 7.5) fed with ethanol and isopropanol, using the simultaneous analyses of 16S rRNA and *dsr*AB gene sequences retrieved from DNA and RNA extracts, and whole-cell hybridization with fluorescently labelled oligonucleotides. Organisms belonging to these two genera were also found using culture-independent methods in the latter study. In addition, we also detected organisms related to the genera *Desulfomicrobium* and *Desulfobacter* in our reactor. These two genera were nei-

Table 1
Carbon, sulphur, iron and zinc content and volatiles by loss on ignition (LOI) results in the solid samples

| Element | % (w/w) | Analytical technique |
|---|---|---|
| C | 7 | LECO |
| S | 21 | LECO |
| Fe | 5 | Acid digestion–ICP |
| Zn | 29 | Acid digestion–ICP |
| LOI | 35 | At 550 °C |

ther found by Kaksonen et al. [5,19] nor by Dar et al. [26]. A *Desulfomicrobium*-related organism was the only SRB maintained in bioreactors working in non-sterile conditions, used to remove Cr(VI) from polluted water and fed with hydrogen [27]; however, this system was initially inoculated with the retrieved *Desulfomicrobium* species. The genus *Desulfomicrobium* also dominated the bacterial communities in a full-scale synthesis gas-fed reactor treating zinc-containing wastewater [28]. *Desulfobacter postagtei* was also found along the column bed in our bioreactor. This organism has a very limited range of usable substrates, but is known to use acetate with a good efficiency [29]. The incomplete oxidation of lactate into acetate probably supported the growth of *Desulfobacter* in our system.

### 3.2. Elemental composition of solids

Table 1 summarizes the results obtained from the bulk solid samples concerning carbon, sulphur, iron and zinc content by different analytical determination techniques. The major part of the carbon content in the solids is expected to be present in the volatile part due to the presence of bacterial cells. Carbon may be also present, but to a lesser extent, in the non-volatile part as carbonate precipitates. Zinc and iron are exclusively present in the non-volatile portion of the solid samples. Sulphur is distributed between zinc and iron sulphide precipitates and elemental sulphur. The results obtained from bulk solid samples by loss on ignition at 550 °C indicate that the content of the volatile part of the solids, attributed mainly to the bacterial cells, has a mean value of 35% (w/w).

### 3.3. Morphology, mineralogy and surface semi-quantitative chemical composition of solids (XRD patterns—SEM–EDX results)

#### 3.3.1. Mineral phases formation

Fig. 3 presents an XRD pattern of a bulk solid sample. The pattern is characterized by the predominance of amorphous phases. Peaks corresponding to iron sulphide, (orthorhombic) marcasite, (face-centered cubic) sphalerite and (hexagonal) wurtzite were also identified. The other peaks appearing on the XRD spectrum have been also identified as different forms of elemental sulphur.

Fig. 4(a) and (b) presents SEM micrographs together with the EDX spectrum (Fig. 4(c)) of a spot on the surface of a sintered glass bead before its use in the SRB reactor as support for biofilm growth. The morphology is characteristic of a highly porous material with pore sizes <100 μm. Silicon and oxygen are exclusively present as expected for sintered glass material.

Fig. 5(a) shows a picture of the column bed glass beads before and after their use in the reactor. The picture shows that, after their use in the reactor, the beads are covered by shiny black solids characteristic of the macroscopic appearance of metal sulphides formed. Fig. 5(b) shows that the solids are also present in the pores of the beads, covering subsurface layers of the beads to a significant extent; the latter being an indication of the formation of very fine particles.

Fig. 6(a) presents a SEM micrograph of a glass bead sampled from the reactor bed. A well-formed crystal with amorphous precipitates on it can be clearly seen. The EDX spectra corresponding to a spot on the crystal surface (Fig. 5(b)) and a spot on the amorphous precipitate (Fig. 5(c)) are also shown. EDX analysis of the crystal surface shows the exclusive presence of Mg, P and O indicating that the crystal is magnesium phos-

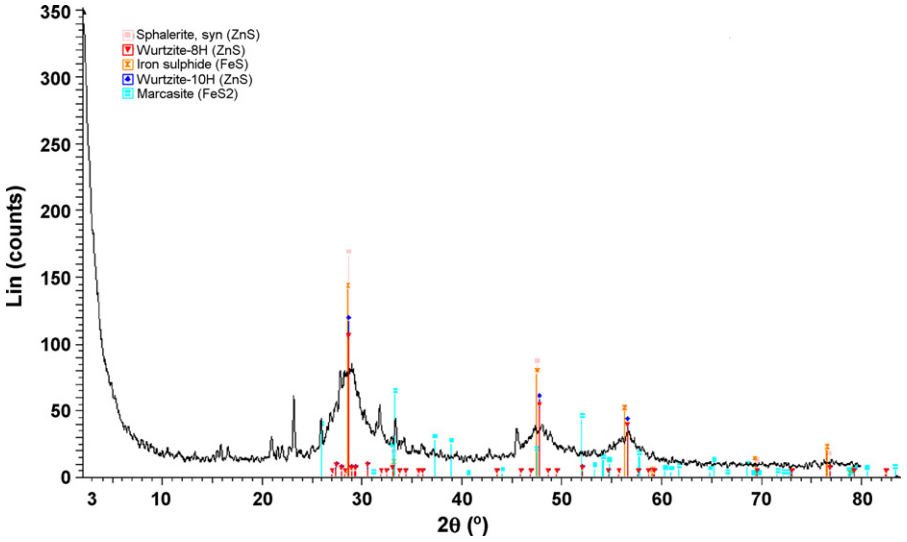


Fig. 3. XRD pattern of a bulk solid sample.

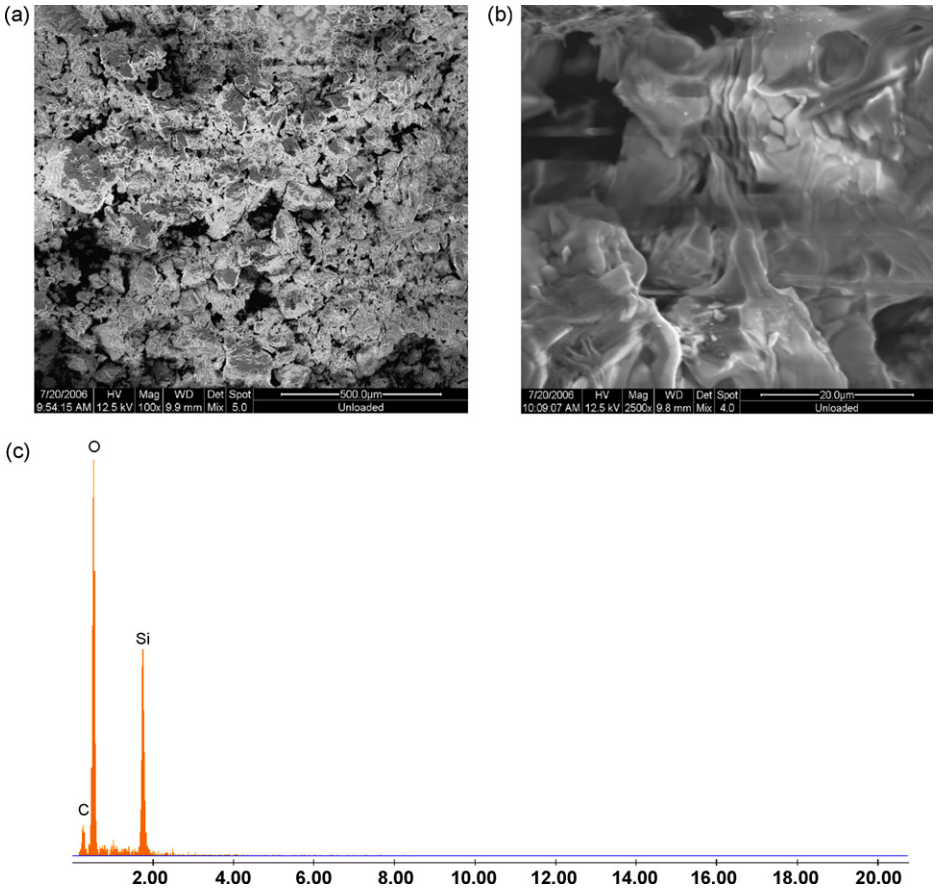


Fig. 4. (a) and (b) SEM pictures (digital mix of LFD and BSE detectors); (c) EDX spectrum of a spot on the surface of a sintered glass bead before its use in the column bed.

phate. EDX analysis of the amorphous precipitates shows that the amorphous phases contain zinc, iron and sulphur.

Fig. 7(a) is a SEM picture of solids retained on a 0.22 μm membrane after filtration of 20 mL of the reactor effluent. The formation of $Mg_3(PO_4)_2$-type crystals on which amorphous solids are precipitated is also obvious from the SEM–EDX presented in Fig. 7(b). Fig. 7(c) presents a detail of Fig. 7(a), accompanied by the EDX spectrum of a spot on the amorphous phases (Fig. 7(d)) confirming the presence of zinc, iron and sulphur on them.

During the operation of the SRB column, the formation of very fine particles was first macroscopically observed (Fig. 5). Rickard and Luther [30] reported the occurrence of amorphous FeS precipitated as subspherical aggregates that were poorly resolved by SEM, suggesting a particle size less than 35 nm. Herbert et al. [11] report the formation and precipitation of fine-grained particles, 100–300 nm in diameter, which have aggregated into "rosettes", 1–2 μm in size, in media containing sulphate-reducing bacteria. Luther and Rickard [31] showed that, in the case of FeS, the first condensed phase is nanoparticulate, metastable mackinawite with a particle size of 2 μm, representing the end of a continuum between aqueous FeS clusters and condensed material. These authors use the Ostwald Step Rule according to which the precipitate with

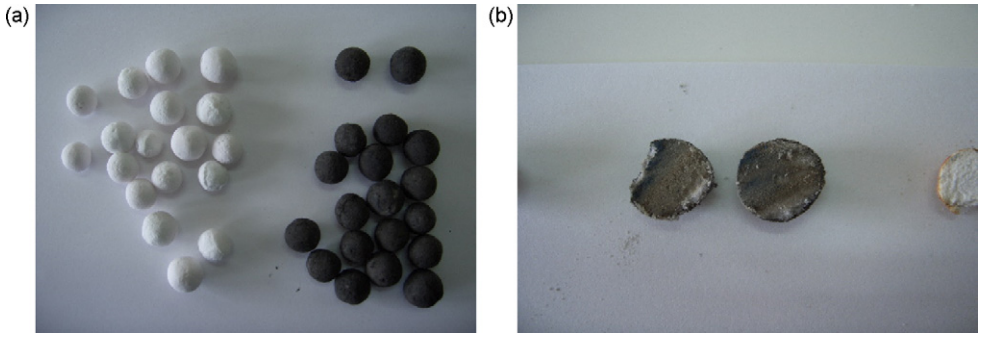


Fig. 5. Picture of the column bed sintered glass beads before and after their use in the reactor (a); dissected sintered glass beads showing the penetration of the submicronic solid particles in subsurface layers (b).

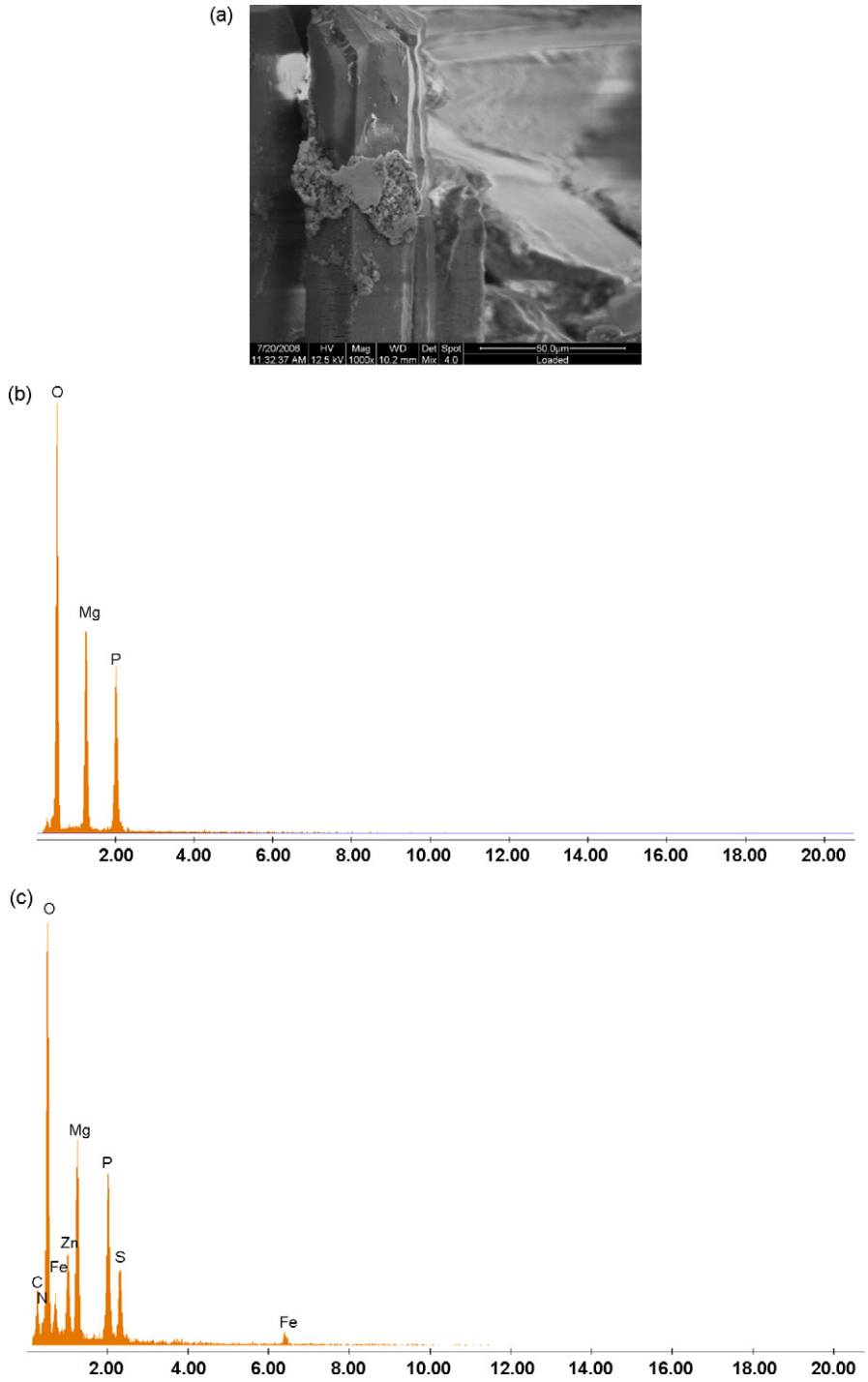


Fig. 6. SEM picture (digital mix of LFD and BSE detectors) of solids on the surface of a sintered glass bead originating from the sulphate-reducing reactor (a). EDX spectra of spots on the surface of the crystal (b) and the amorphous solids (c).

the highest solubility (i.e. the least stable solid phase) will form first in a consecutive precipitation reaction, suggesting that mineral formation occurs via precursors (intermediates) that can be recognized at the molecular level. Metal sulphide species yield quantum size clusters with metals Fe, Zn, Cu, Cd and Pb. These quantum-sized materials are also termed molecular clusters that consist of an indefinite number of molecular units with a defined stoichiometry. These clusters, represented by the general formulae $MeS_{aq}$, form rapidly and appear to be formed with stoichiometries $Me_2S_2$ for Fe and $Me_3S_3$, $Me_4S_4$ and $Me_4S_6$ for Zn, Cu, Pb and Ag. They are of remarkable stability and of sizes of the order of 0.5–1 nm. These stoichiometries are not exceeded at low metal and sulphide concentrations (<2 μM). At higher metal and sulphide concentrations (>10 μM), aggregation to higher ordered nano-crystalline particles occurs. The monomeric units of Fe and Zn sulphide clusters also lead to nano-crystalline materials.

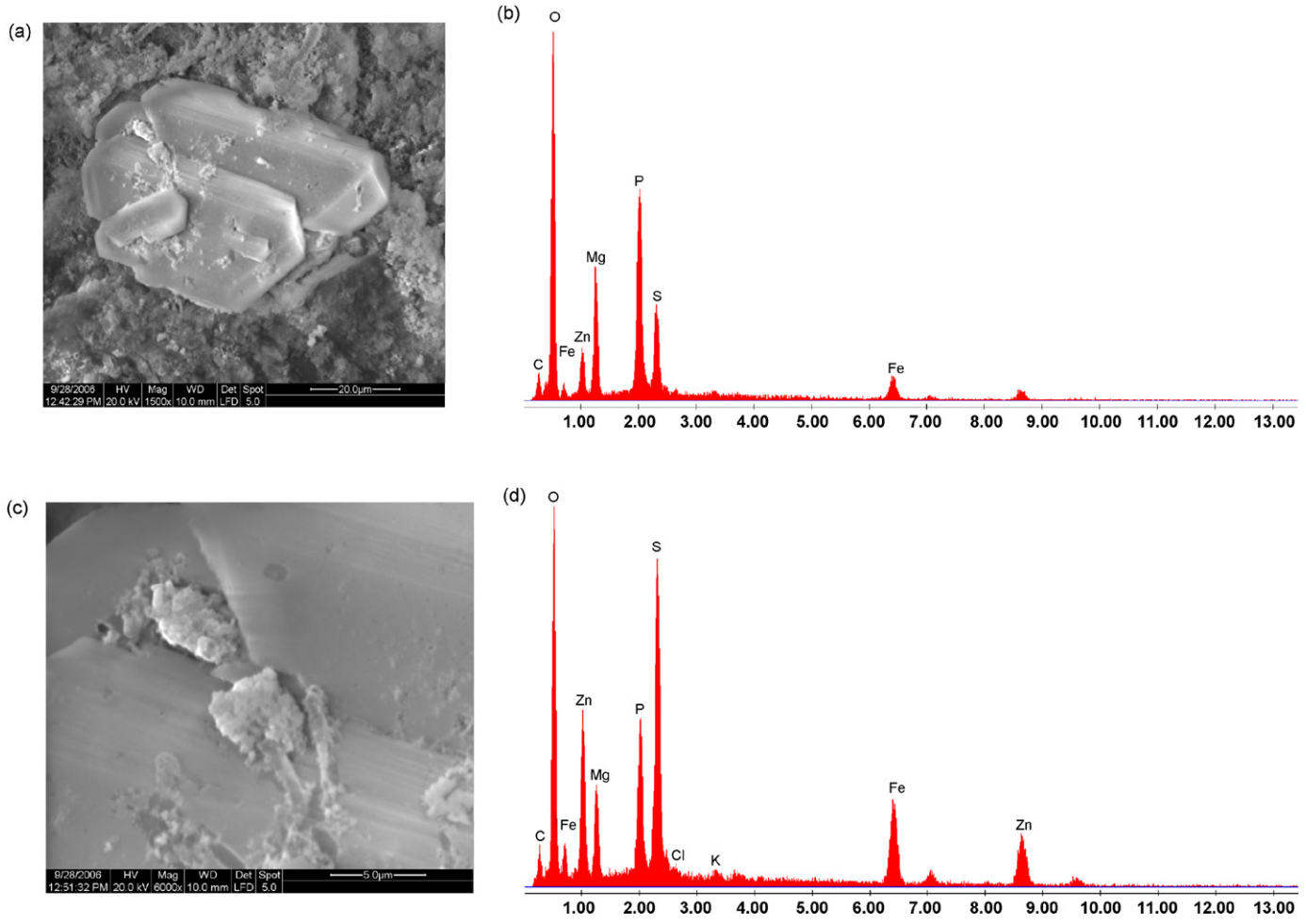


Fig. 7. SEM picture (LFD detector) of solids retained on a 0.22 μm membrane where amorphous precipitates can be seen on well-formed crystals (a); the EDX spectrum of a spot on the crystal surface shows the presence of Mg, P, O together with Zn, Fe and S (b); detail of (a), (c); EDX spectrum of a spot on the amorphous solids (d). Zn, Fe and S seem to be predominant.

As far as zinc is concerned, Zn(II) exists in aqueous solution as the hexaaquo $Zn(H_2O)_6^{2+}$ ion, with Zn in octahedral coordination [32]. The stable ZnS phase, sphalerite, occurs as infinitely repeating series of ZnS units with both Zn and S in tetrahedral coordination [33]. To get from one state to the other, a series of reactions must occur between the Zn(II) and S(−II) species promoting the initial substitution of water by sulphide. Reaction intermediates then form that condense and the coordination of both Zn and S changes. The process is further complicated by the release of protons, because S(−II) does not have any significant activity in aqueous solutions. The product is an amorphous ZnS that develops a preferred structure, usually sphalerite but often with a trace of its metastable dimorph, wurtzite [34]. The $Zn_4S_6$ cluster is structurally analogous to ZnS minerals (particularly sphalerite) and is a viable precursor to mineral formation [34]. In the present study, the presence of the solids into the pores of the sintered glass beads (Fig. 5), the results obtained by XRD (Fig. 3), the amorphous aggregates and their composition shown by SEM–EDX (Figs. 6 and 7) are explained and supported by the findings summarized above.

The results obtained by XRD (Fig. 3) and SEM–EDX (Figs. 6 and 7) show that the amorphous phases are composed of zinc, iron and sulphur. Iron sulphide, marcasite, sphalerite and wurtzite are also present but in a lesser extent (Fig. 3). The predominance of the amorphous phases is also reported by other authors [11] who point out that precipitates formed in media containing sulphate-reducing bacteria are poorly crystalline iron monosulphides exhibiting incipient crystallization towards mackinawite.

For the operating conditions of the SRB column, mainly the anaerobic environment and the temperature of 22 °C, the predominance of amorphous iron and zinc sulphides can be further analyzed as follows. The nucleation of $FeS_2$ is extremely slow below 100 °C. Instead of $FeS_2$ nuclei, the reaction of ferrous ions and polysulphide ions produces initially amorphous FeS. Below 100 °C, the conversion of amorphous FeS to $FeS_2$ proceeds at a significant rate only if intermediate sulphur species are present (i.e. polysulphides, polythionates or thisulphate). In the absence of any sulphur contributor or with only hydrogen sulphide or bisulphide present, the conversion of amorphous FeS to $FeS_2$ proceeds at an insignificant rate [35,36]. The grain size

of the final products depends on the pH [36]. The grain size decreases with increasing pH. Below pH 4 the individual grains are 2–5 μm, whereas above pH 6 the individual particles range from 0.1 to 2 μm [36]. In the environment of the SRB column, the solution pH shifts progressively from the initial value of 3–4 (influent) to a final value of ca. 8.8 as the solution flows out of the column. The pH is usually stabilized at a value around 8 within the first 10 cm of the column bed [20]. Under these conditions the formation of the observed very fine particles is explained.

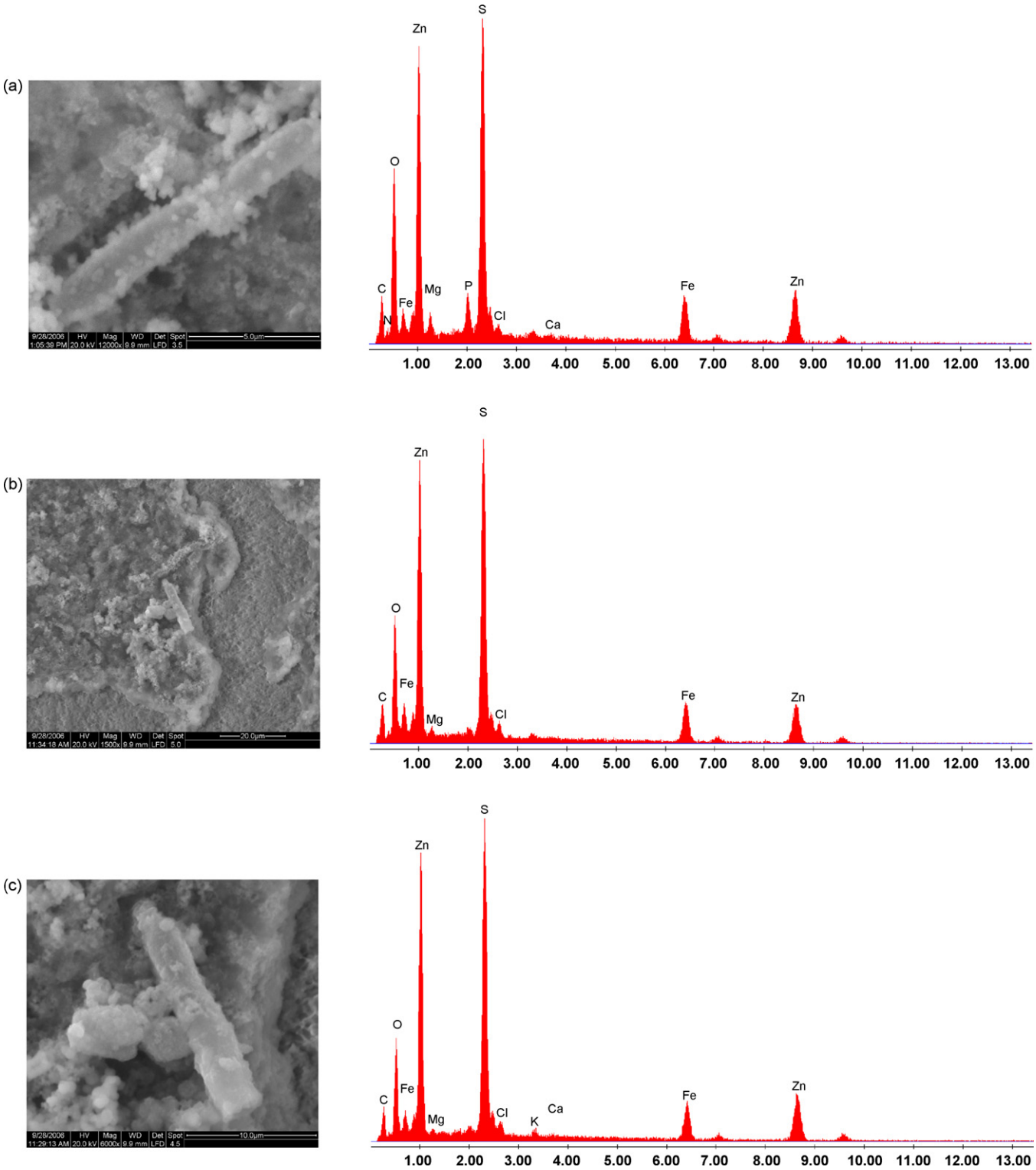


Fig. 8. Rod-shaped solids with hazy surfaces and length of about 10 μm (a), (b) and (c, zoom of b). The corresponding EDX spectra, presented beside each picture, show the predominance of zinc, iron and sulphur.

The conversion rate of amorphous to crystalline phases is also dependent on the oxidation state and increases with an increase in oxidation state. Intermediate sulphur species (i.e. polysulphides, polythionates or thiosulphate) are not expected to be abundant under strongly reducing conditions. Thus, the conversion of amorphous to crystalline phases is not favoured by the reducing environment of the SRB column [36].

In summary, the predominance of the amorphous phases of zinc and iron sulphides and the formation of very fine particles observed during the operation of the SRB column in the present study, are in agreement and can be explained by the formation procedures of metal sulphides at ambient temperature, alkaline pH and reducing conditions described above.

Consequences of the predominance of amorphous phases of metal sulphides for the fate of the produced sludge may mainly be alterations due to natural weathering, i.e. oxidation (crystalline phases are less susceptible to such alterations) in case of disposal. However, the sludge consisting mainly of amorphous phases of metal sulphides, may be more easily processed for metal recovery.

### *3.3.2. Bacterial cells encapsulation by metal sulphides*

Fig. 8(a) and (b) presents rod-shaped solids with hazy surfaces and length of about 10 μm, Fig. 8(c) being a further magnification of Fig. 8(b). EDX analysis of their surface, also presented in the same figure, suggests the predominance of zinc, iron and sulphur.

These rod-shaped solids may be bacterial cells encapsulated by zinc and iron sulphides as it is confirmed by the composition resulting from the EDX analysis of the spots on their surfaces. Reports of similar results [12] indicate that bacterial cell walls appear to be encapsulated by a cloudy haze due to the deposition of metal sulphides on the cell wall surface and/or in the vicinity of the bacterial cells. As a consequence, the solids formed hinder the bacterial metabolism by preventing the contact between the reactants (sulphate–organic matter) and the necessary enzymes. This was described by Utgikar et al. [12] as the inhibitory effect/mechanism of metal sulphides formation on SRB cultures. However, such an inhibitory effect did not seem to be pronounced during 1 year of continuous operation of the SRB column as suggested from the results of total zinc, iron and sulphate removal from the liquid phase treated in the reactor [20]. Especially, during the last period of the reactor operation (i.e. at the end of the 310-day period), the reactor operated with initial Zn concentration of 400 mg/L and complete removal of zinc was obtained for the reactor effluent [20]. This can be attributed to the capacity of the fixed bed column to support the continuous development of biofilm on the provided very high-specific area. Increased cell density allows the continuous release of hydrogen sulphide and the formation of extracellular precipitates of metal sulphides as shown in Figs. 6 and 7. Even if part of the bacterial population is inactivated via encapsulation by metal sulphides as shown in Fig. 8, the further growth and proliferation of the biomass on the provided support allows the observed efficient operation of the reactor for extended operating periods.

## 4. Conclusions

The following conclusions can be drawn by the present study:

1. A diverse population of δ-*Proteobacteria* SRB affiliated to four distinct genera, namely *Desulfomicrobium*, *Desulfobacter*, *Desulfobulbus* and *Desulfovibrio*, colonized the system. Molecular fingerprints of 16S rRNA genes were highly reproducible during time, as well as at different location along the column bed, indicating that the community, although complex, had reached a steady state at that period of the process.
2. Extracellular formation of amorphous zinc and iron sulphides predominates during the operation of the sulphate-reducing reactor as shown by both XRD and SEM–EDX analyses.
3. The formation of very fine particles and the predominance of amorphous zinc and iron sulphides is the likely result of the reactor operating conditions primarily of the ambient temperature, the reducing environment and the alkaline pH.
4. Bacterial cells become encapsulated by zinc and iron sulphides as observed by SEM–EDX. However, any metal precipitation inhibition due to the inactivation of bacterial cells by the metal sulphides precipitates was overcome by the regeneration capacity of the bacterial population of the reactor over the increased area of the provided support.

## Acknowledgements

This work was supported by BIOMINE, EU 6th Framework Project (Contract No. 500329). The authors thank Dr. V. Lymperopoulou and K. Balta (School of Chemical Engineering, NTUA) for technical assistance with SEM–EDX analysis.

## References

[1] D.H. Dvorak, R.S. Hedin, H.M. Edenborn, P.E. McIntire, Treatment of metal-contaminated water using bacterial sulfate reduction: results from pilot-scale reactors, Biotechnol. Bioeng. 40 (5) (1992) 609–616.
[2] S. Foucher, F. Battaglia-Brunet, I. Ignatiadis, D. Morin, Treatment by sulfate-reducing bacteria of Chessy acid-mine drainage and metals recovery, Chem. Eng. Sci. 56 (4) (2001) 1639–1645.
[3] A.H. Kaksonen, P.D. Franzmann, J.A. Puhakka, Performance and ethanol oxidation kinetics of a sulfate-reducing fluidized-bed reactor treating acidic metal-containing wastewater, Biodegradation 14 (3) (2003) 207–217.
[4] A.H. Kaksonen, P.D. Franzmann, J.A. Puhakka, Effects of hydraulic retention time and sulfide toxicity on ethanol and acetate oxidation in sulfate-reducing metal-precipitating fluidized-bed reactor, Biotechnol. Bioeng. 86 (3) (2004) 332–343.
[5] A.H. Kaksonen, J.J. Plumb, P.D. Franzmann, J.A. Puhakka, Simple organic electron donors support diverse sulfate-reducing communities in fluidized-bed reactors treating acidic metal- and sulfate-containing wastewater, FEMS Microbiol. Ecol. 47 (3) (2004) 279–289.
[6] A.H. Kaksonen, M.L. Riekkola-Vanhanen, J.A. Puhakka, Optimization of metal sulphide precipitation in fluidized-bed treatment of acidic wastewater, Water Res. 37 (2) (2003) 255–266.
[7] L.W. Hulshoff, P.N.L. Lens, J. Weijma, A.J.M. Stams, New developments in reactor and process technology for sulfate reduction, Water Sci. Technol. 44 (8) (2001) 67–76.
[8] S. Riesen, J.L. Huisman, G. Schouten, Ecotoxicity: an important (new) parameter for sustainability in metallurgy, in: Proceedings of the 16th Inter-

national Biohydrometallurgy Symposium, IBS 2005, Cape Town, South Africa, 2005.
[9] J.R. Postgate, Recent advances in the study of the sulfate-reducing bacteria, Bacteriol. Rev. 29 (4) (1965) 425–441.
[10] G. Zellner, F. Neudorfer, H. Diekmann, Degradation of lactate by an anaerobic mixed culture in a fluidized-bed reactor, Water Res. 28 (6) (1994) 1337–1340.
[11] R.B. Herbert, S.G. Benner, A.R. Pratt, D.W. Blowes, Surface chemistry and morphology of poorly crystalline iron sulfides precipitated in media containing sulfate-reducing bacteria, Chem. Geol. 144 (1–2) (1998) 87–97.
[12] V.P. Utgikar, S.M. Harmon, N. Chaudhary, H.H. Tabak, R. Govind, J.R. Haines, Inhibition of sulfate-reducing bacteria by metal sulfide formation in bioremediation of acid mine drainage, Environ. Toxicol. 17 (1) (2002) 40–48.
[13] M.D. Tucker, L.L. Barton, B.M. Thomson, Reduction of Cr, Mo, Se and U by desulfovibrio desulfuricans immobilized in polyacrylamide gels, J. Ind. Microbiol. Biotechnol. 20 (1) (1998) 13–19.
[14] K.H. Lanouette, Heavy metals removal, Chem. Eng. 84 (21) (1977) 73–80.
[15] B.E. Rittmann, P.L. McCarty, Environmental Biotechnology: Principles and Applications, McGraw-Hill, 2001.
[16] E. Remoudaki, A. Hatzikioseyian, P. Kousi, M. Tsezos, The mechanism of metals precipitation by biologically generated alkalinity in biofilm reactors, Water Res. 37 (16) (2003) 3843–3854.
[17] J.S. Whang, D. Young, M. Pressman, Soluble-sulfide precipitation for heavy metals removal from wastewaters. Engineering details of a treatment plant scheduled to be operational in September 1981, Environ. Prog. 2 (1) (1982) 110–113.
[18] H.H. Tabak, R. Scharp, J. Burckle, F.K. Kawahara, R. Govind, Advances in biotreatment of acid mine drainage and biorecovery of metals. 1. Metal precipitation for recovery and recycle, Biodegradation 14 (6) (2003) 423–436.
[19] A. Kaksonen, J. Plumb, W. Robertson, P. Franzmann, J. Gibson, J. Puhakka, Culturable diversity and community fatty acid profiling of sulfate-reducing fluidized-bed reactors treating acidic metal-containing wastewater, Geomicrobiol. J. 21 (7) (2004) 469–480.
[20] P. Kousi, E. Remoudaki, A. Hatzikioseyian, M. Tsezos, A study of the operating parameters of a sulphate-reducing fixed-bed reactor for the treatment of metal-bearing wastewater, Adv. Mater. Res. 20/21 (2007) 230–234.
[21] C. Delbès, R. Moletta, J.-J. Godon, Bacterial and archaeal 16S rDNA and 16S rDNA dynamics during an acetate crisis in an anaerobic digestor ecosystem, FEMS Microbiol. Ecol. 35 (2001) 19–26.
[22] D. Benson, M.S. Bogusk, D.J. Lipman, J. Ostell, B.F. Ouellette, B.A. Rapp, D.L. Wheeler, GenBank, Nucleic Acids Res. 27 (1999) 12–17.
[23] T.A. Hall, BioEdit: a user-friendly biological sequence alignment editor and analysis program for Windows 95/98/NT, Nucleic Acids Symp. Ser. 41 (1999) 95–98.
[24] M. Kimura, A simple model for estimating evolutionary rates of base substitutions through comparative studies of nucleotide sequences, J. Mol. Evol. 16 (1980) 111–120.
[25] J.G. Holt, N.R. Krieg, P.H.A. Sneath, J.T. Staley, S.T. Williams, Bergey's Manual of Determinative Bacteriology, 9th ed., Williams & Wilkins, Baltimore, Maryland, 1994.
[26] S.A. Dar, L. Yao, U. van Dongen, J.G. Kuenen, G. Muyzer, Analysis of diversity and activity of sulfate-reducing bacterial communities in sulfidogenic bioreactors using 16S rRNA and *dsr*B genes as molecular markers, Appl. Environ. Microbiol. 73 (2) (2007) 594–604.
[27] F. Battaglia-Brunet, C. Michel, C. Joulian, B. Ollivier, I. Ignatiadis, Relationship between sulphate starvation and chromate reduction in a $H_2$-fed fixed-film bioreactor, Water Air Soil Pollut. (2007) (published online).
[28] B.H.G.W. van Houten, K. Roest, V.A. Tzeneva, H. Dijkman, H. Smidt, A.J.M. Stams, Occurrence of methanogenesis during start-up of a full-scale synthesis gas-fed reactor treating sulfate and metal-rich wastewater, Water Res. 40 (3) (2006) 553–560.
[29] K. Ingvorsen, A.J.B. Zehnder, B.B. Jorgensen, Kinetics of sulfate and acetate uptake by desulfobacter postgatei, Appl. Environ. Microbiol. 47 (2) (1984) 403–408.
[30] D. Rickard, G.W. Luther, Kinetics of pyrite formation by the $H_2S$ oxidation of iron(II) monosulfide in aqueous solutions between 25 and 125 °C: the mechanism, Geochim. Cosmochim. Acta 61 (1) (1997) 135–147.
[31] G.W. Luther, D.T. Rickard, Metal sulfide cluster complexes and their biogeochemical importance in the environment, J. Nanopart. Res. V7 (4) (2005) 389–407.
[32] N.N. Greenwood, A.C. Earnshaw, Chemistry of the Elements, 1st ed., Pergamon Press, 1984.
[33] A.F. Wells, Structural Inorganic Chemistry, 5th ed., Clarenton, 1986.
[34] G.W. Luther, S.M. Theberge, D.T. Rickard, Evidence for aqueous clusters as intermediates during zinc sulfide formation, Geochim. Cosmochim. Acta 63 (19–20) (1999) 3159–3169.
[35] M.A.A. Schoonen, H.L. Barnes, Reactions forming pyrite and marcasite from solution. I. Nucleation of $FeS_2$ below 100 °C, Geochim. Cosmochim. Acta 55 (6) (1991) 1495–1504.
[36] M.A.A. Schoonen, H.L. Barnes, Reactions forming pyrite and marcasite from solution. II. Via FeS precursors below 100 °C, Geochim. Cosmochim. Acta 55 (6) (1991) 1505–1514.